

# Time correlation between the radio and gamma-ray activity in blazars and the production site of the gamma-ray emission

W. Max-Moerbeck,<sup>1,2★</sup> T. Hovatta,<sup>1,3</sup> J. L. Richards,<sup>4</sup> O. G. King,<sup>1</sup> T. J. Pearson,<sup>1</sup>  
A. C. S. Readhead,<sup>1</sup> R. Reeves,<sup>1,5</sup> M. C. Shepherd,<sup>1</sup> M. A. Stevenson,<sup>1</sup> E. Angelakis,<sup>6</sup>  
L. Fuhrmann,<sup>6</sup> K. J. B. Grainge,<sup>7</sup> V. Pavlidou,<sup>1,6,8</sup> R. W. Romani<sup>9</sup> and J. A. Zensus<sup>6</sup>

<sup>1</sup>Cahill Center for Astronomy and Astrophysics, California Institute of Technology, Pasadena, CA 91125, USA

<sup>2</sup>National Radio Astronomy Observatory (NRAO), PO Box 0, Socorro, NM 87801, USA

<sup>3</sup>Aalto University Metsähovi Radio Observatory, Metsähovintie 114, FI-02540 Kylmäla, Finland

<sup>4</sup>Department of Physics, Purdue University, West Lafayette, IN 47907, USA

<sup>5</sup>Departamento de Astronomía, Universidad de Concepción, Casilla 160-C, Concepción, Chile

<sup>6</sup>Max-Planck-Institut für Radioastronomie, Auf dem Hügel 69, D-53121 Bonn, Germany

<sup>7</sup>Jodrell Bank Centre for Astrophysics, School of Physics and Astronomy, The University of Manchester, M13 9PL, UK

<sup>8</sup>Department of Physics, University of Crete/Foundation for Research and Technology-Hellas, Heraklion GR-71003, Greece

<sup>9</sup>W. W. Hansen Experimental Physics Laboratory, Kavli Institute for Particle Astrophysics and Cosmology, Department of Physics and SLAC National Accelerator Laboratory, Stanford University, Stanford, CA 94305, USA

Accepted 2014 August 26. Received 2014 August 21; in original form 2014 June 20

## ABSTRACT

In order to determine the location of the gamma-ray emission site in blazars, we investigate the time-domain relationship between their radio and gamma-ray emission. Light curves for the brightest detected blazars from the first 3 yr of the mission of the *Fermi Gamma-ray Space Telescope* are cross-correlated with 4 yr of 15 GHz observations from the Owens Valley Radio Observatory 40 m monitoring programme. The large sample and long light-curve duration enable us to carry out a statistically robust analysis of the significance of the cross-correlations, which is investigated using Monte Carlo simulations including the uneven sampling and noise properties of the light curves. Modelling the light curves as red noise processes with power-law power spectral densities, we find that only one of 41 sources with high-quality data in both bands shows correlations with significance larger than  $3\sigma$  (AO 0235+164), with only two more larger than even  $2.25\sigma$  (PKS 1502+106 and B2 2308+34). Additionally, we find correlated variability in Mrk 421 when including a strong flare that occurred in 2012 July–September. These results demonstrate very clearly the difficulty of measuring statistically robust multiwavelength correlations and the care needed when comparing light curves even when many years of data are used. This should be a caution. In all four sources, the radio variations lag the gamma-ray variations, suggesting that the gamma-ray emission originates upstream of the radio emission. Continuous simultaneous monitoring over a longer time period is required to obtain high significance levels in cross-correlations between gamma-ray and radio variability in most blazars.

**Key words:** galaxies: active – BL Lacertae objects: general – quasars: general – gamma rays: galaxies – radio continuum: galaxies.

## 1 INTRODUCTION

Blazars are active galactic nuclei (AGN) with jets closely aligned to the line of sight (e.g. Blandford & Konigl 1979). They are the most numerous class of sources detected in the GeV band by the Large

Area Telescope (LAT) on the *Fermi Gamma-ray Space Telescope* (Ackermann et al. 2011b). Blazars have double-peaked broad-band spectral energy distributions and show strong variability from radio to gamma-rays (e.g. von Montigny et al. 1995). It is accepted that the low-energy emission is produced by synchrotron radiation from electrons within the jet, while the high-energy gamma-ray emission is produced by inverse-Compton scattering of a soft photon field by the same electrons (e.g. Jones, O'dell & Stein 1974; Dermer

★ E-mail: wmax@nrao.edu

& Schlickeiser 1993; Sikora, Begelman & Rees 1994; Błażejowski et al. 2000) or by hadronic processes (e.g. Mannheim & Biermann 1992). That a common mechanism regulates the luminosity at high and low energies is demonstrated by the correlation between the mean radio flux density and mean gamma-ray flux (Kovalev et al. 2009; Mahony et al. 2010; Nieppola et al. 2011). Ackermann et al. (2011a) and Pavlidou et al. (2012) showed that this correlation is not an effect of distance modulation of the fluxes.

The location of the gamma-ray emission site in blazars is not yet known. Gamma-rays may be produced, for example, in the radio-emitting regions (e.g. Jorstad et al. 2001), or much closer to the central engine (e.g. Blandford & Levinson 1995). Radio observations with milliarcsecond resolution have resolved the radio-emitting regions and measured outflow velocities, but at high energies the angular resolution is insufficient and we must infer the size and location of the emission regions from flux variations. If gamma-ray and radio emission are triggered by shocks propagating along a relativistic jet, the time delay between flares in the two bands depends on their separation. Several studies have found time-lagged correlation between these two energy bands, but without a large sample with well-sampled light curves it is difficult to assess the significance of the correlations (e.g. Marscher et al. 2008; Abdo et al. 2010a; Agudo et al. 2011a,b). In a statistical study of 183 bright *Fermi*-detected sources, Pushkarev, Kovalev & Lister (2010) found that, on average, radio flares occur later than gamma-ray flares. A more recent investigation using multiple radio frequencies and longer light curves (Fuhrmann et al. 2014) also found correlated radio and gamma-ray variability with a frequency-dependent radio lag.

In comparing multiwavelength light curves of individual blazars over short time periods, claims are often made for correlations but the actual significance is rarely computed. To remedy this situation and search for the existence of significant correlations and their physical origin, we have undertaken a long-term radio monitoring campaign of a large number of blazars. We apply robust statistical methods to estimate the significance of correlations and find that most of the blazars in our sample only show correlations below  $2.25\sigma$ . Only three out of 41 objects show correlations above a  $2.25\sigma$  level where we expect to find one random uncorrelated source to appear, with only one above the  $3\sigma$  level of significance. Thus, it is clear that establishing a statistically significant cross-correlation is more difficult than is generally assumed. We also provide a tentative interpretation for the origin of the time lag and the location of the gamma-ray emission site.

## 2 OBSERVATIONS

Through our Owens Valley Radio Observatory (OVRO) 40 m programme, twice per week we observe all sources in the Candidate Gamma Ray Blazar Survey (Healey et al. 2008) and the blazars detected in the *Fermi*-LAT AGN catalogues (Abdo et al. 2010b; Ackermann et al. 2011b) north of declination  $-20^\circ$  at 15 GHz. This sample has a total of 1593 sources, of which 685 have gamma-ray detections, with 454 and 634 in the first and second *Fermi*-LAT AGN catalogues, respectively.

Radio observations from 2008 January 1 to 2012 February 26 are included in this study. The radio flux density measurements have a thermal noise floor of  $\sim 5$  mJy with an additional 2 per cent contribution from pointing errors. The flux density scale is determined from regular observations of 3C 286 assuming the Baars et al. (1977) value of 3.44 Jy at 15.0 GHz, giving a 5 per cent overall scale accuracy. A detailed discussion of the observing strategy and

calibration procedures can be found in Richards et al. (2011). The radio light curves have different characteristics, with a mean and standard deviation for length  $1178 \pm 441$  d, number of data points  $195 \pm 88$ , and average sampling  $6.4 \pm 1.4$  d. The light curves of the cases discussed in this paper are shown in Fig. 1. The monitoring programme is ongoing and all the light curves are made public on the programme website.<sup>1</sup>

The LAT is a pair-conversion gamma-ray telescope, sensitive to photon energies from about 20 MeV up to  $>300$  GeV, that observes the whole sky once every three hours (Atwood et al. 2009). *Fermi*-LAT light curves with 7 d time bins from 2008 August 4 through 2011 August 12 were produced for 86 sources detected in at least 75 per cent of monthly time bins (Nolan et al. 2012). We use an unbinned likelihood analysis, with source spectral models and positions from Ackermann et al. (2011b). We froze the sources spectral parameters (including the target) and let only the flux vary in sources within  $10^\circ$  of the target. We use *Fermi*-LAT ScienceTools-v9r23p1 with P7\_V6 source event selection and instrument response functions, diffuse models `gal_2yearp7v6_v0.fits` and `iso_p7v6source.txt`, only photons with zenith angle  $< 100^\circ$  and other standard data cuts and filters (e.g. Abdo et al. 2011).<sup>2</sup> We use a region of interest of  $10^\circ$  radius and a source region of  $15^\circ$  radius. Photon integral fluxes from 100 MeV to 200 GeV are reported when the test statistic<sup>3</sup>  $TS \geq 4$ , and  $2\sigma$  upper limits when  $TS < 4$  ( $\sim 30$  per cent of the data).

## 3 TIME LAGS AND THEIR SIGNIFICANCE

The radio light curves are sampled unevenly due to weather and other problems. The gamma-ray light curves are weekly averages, but some measurements are upper limits ( $\sim 30$  per cent of the data) that are ignored in this analysis. We tested the possible effect of ignoring upper limits by using the best flux estimate independent of TS and the upper limit itself as a flux, obtaining comparable results in all cases, thus showing that it is safe to ignore upper limits for this sample of bright sources. The cross-correlation is measured using the discrete cross-correlation function (DCF; Edelson & Krolik 1988), with local normalization (Welsh 1999), also known as local cross-correlation function (LCCF). We find that the LCCF results in a greater detection efficiency for known correlations injected in simulated data. We estimate the cross-correlation significance with Monte Carlo simulations that assume a simple power-law power spectral density model for the light curves ( $PSD \propto 1/f^\beta$ ), motivated by previous work (e.g. Hufnagel & Bregman 1992; Edelson et al. 1995; Uttley et al. 2003; Arévalo et al. 2008; Chatterjee et al. 2008; Abdo et al. 2010c). We simulate a large number of independent, uncorrelated light-curve pairs that replicate the sampling, measurement error distribution, and statistical properties of the observations, using the method of Timmer & Koenig (1995). From the distribution of cross-correlations at each time lag, we estimate the chance probability of obtaining a given correlation value. The method is described in detail by Max-Moerbeck et al. (2014).

For 13 sources where a PSD fit is possible in both bands, we use the best-fitting power-law index values; for the others, we use

<sup>1</sup> <http://astro.caltech.edu/ovroblazars/>

<sup>2</sup> Science Tools, LAT data, and diffuse emission models are available from the *Fermi* Science Support Center, <http://fermi.gsfc.nasa.gov/ssc>

<sup>3</sup> The test statistic is a measure of detection significance, defined as  $TS = 2\Delta\log(\text{likelihood})$  between models with and without the source (Mattox et al. 1996).

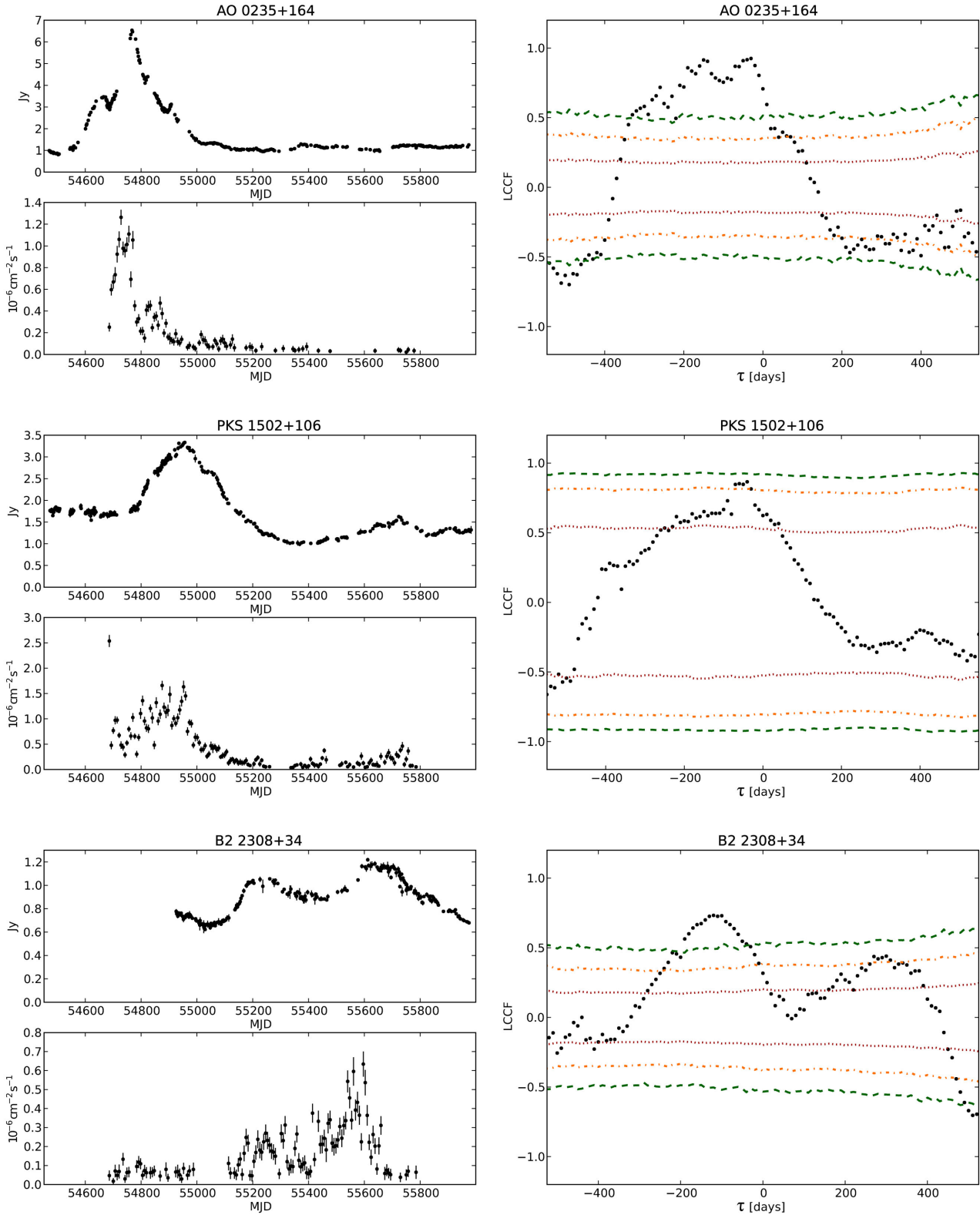


**Figure 1.** Light curves (left) and cross-correlation (right) for sources with significant cross-correlation. Contours indicate the cross-correlations significances (red dotted line:  $1\sigma$ ; orange dash-dotted line:  $2\sigma$ ; green dashed line:  $3\sigma$ ). The most significant peak for AO 0235+164 is at  $-150 \pm 8$  d with 99.99 per cent significance, for PKS 1502+106 it is at  $-40 \pm 13$  d with 98.09 per cent significance for the best-fitting PSD model and 97.54 per cent for the lower limit, and for B2 2308+34 it is at  $-120 \pm 14$  d with 99.99 per cent significance for the best-fitting PSD model and 99.33 per cent for the lower limit. The significance lower limit for PKS 1502+106 is above the 97.56 per cent threshold within the error (see Table 1).

population-average values as described below. We characterize the PSDs using a modified implementation of Uttley, McHardy & Papadakis (2002) that uses sampling window functions to reduce red-noise leakage. The effects of uneven sampling are incorporated by comparing the observed PSD to those derived from simulated light curves. We compute the PSD from the data and obtain a mean PSD with scatter from simulated light curves for several values of the power-law index. The best fit is found by comparing the PSD from the data with the simulated ones using a  $\chi^2$  test. We find good constraints for the radio PSD power-law index for 43 sources (Table 1). The distribution of indices is clustered around 2.3, with a typical error of 0.4, and is consistent with a single value equal to the sample mean of  $2.3 \pm 0.1$ . We adopt a value of  $\beta_{\text{radio}} = 2.3$  for sources with no fitted radio PSD. In the gamma-ray band, the PSD power-law index is constrained for 29 sources. The distribution has peaks at about 0.5 and 1.6. The peak at 1.6 is consistent with results for the brightest sources from Abdo et al. (2010c) ( $1.4 \pm 0.1$  for flat spectrum radio quasars (FSRQs) and  $1.7 \pm 0.3$  for BL Lacs) but steeper than that found in Ackermann et al. (2011b) (about 1.15 for the average PSD of the brightest blazars). For sources with no gamma-ray PSD fit, we assume  $\beta_\gamma = 1.6$  which gives conservative estimates of the cross-correlation significance.

#### 4 RESULTS OF THE CROSS-CORRELATION SIGNIFICANCE

We estimated the cross-correlation between the radio and gamma-ray light curves and its significance for 41 of the 86 sources. 23 are excluded for being non-variable at the  $3\sigma$  level (a  $\chi^2$  test of the null hypothesis of constant flux shows that the observed variations are consistent with observational noise). We also exclude ‘noisy’ light curves where more than 1/3 of the variance comes from observational noise. We also exclude light curves consistent with a linear trend in the overlapping section; for such sources, longer light curves are needed to probe the relevant time-scales. These two restrictions eliminate 22 more objects.

To include the effects of red-noise leakage and aliasing, we simulate 10 yr light-curves with a 1 d time resolution. The cross-correlation is estimated for independent bins of 10 d. In each case, we simulate 20 000 independent light-curve pairs using the appropriate PSD (Section 3 and Table 1). To eliminate spurious correlations, we restrict the time-lag search interval to  $\pm 0.5$  times the length of the shortest light curve. For each source, the position and significance of the most significant cross-correlation peak are given in Table 1. The peak position uncertainty is estimated by ‘flux randomization’ and ‘random subset selection’ (Peterson et al. 1998). The error on the significance is determined using a bootstrap method (Max-Moerbeck et al. 2014). We set the significance threshold at 97.56 per cent ( $2.25\sigma$ ), at which we expect to have one object with a chance high correlation.

At this threshold, three of our 41 sources show interesting levels of correlation: AO 0235+164,  $\tau = -150 \pm 8$  d with 99.99 per cent significance (the only case with significance  $\geq 3\sigma$ ); PKS 1502+106,  $\tau = -40 \pm 13$  d with 97.54 per cent significance;<sup>4</sup> and B2 2308+34,  $\tau = -120 \pm 14$  d with 99.33 per cent significance. The results are presented in Fig. 1, where a negative lag indicates that radio variations occur after gamma-ray variations.

Significant correlated variability has been reported by Agudo et al. (2011b) for AO 0235+164, with a delay of about  $-30$  d using radio data up to MJD 55000. With our longer light curves, we find a significant correlation at a delay of  $-150$  d, although the cross-correlation peak is broad and there is a second peak of comparable amplitude and significance at  $-30$  d. This adds a large uncertainty when considered in the estimation of the location of the gamma-ray emission site because our current data cannot discriminate between these two peaks. No significant cross-correlations have been previously reported for PKS 1502+106 or B2 2304+34.

#### 5 THE CASE OF MRK 421

A major radio flare was observed from Mrk 421 on 2012 September 21, when its 15 GHz flux density reached  $1.11 \pm 0.03$  Jy, approximately 2.5 times its previous median value (Hovatta et al. 2012). On 2012 July 16, the source was detected at its highest level to date by *Fermi*-LAT. Its integrated photon flux for  $E > 100$  MeV was  $(1.4 \pm 0.2) \times 10^{-6}$  ph cm $^{-2}$  s $^{-1}$ , a factor of 8 greater than the average in the second *Fermi*-LAT catalogue (D’Ammando & Orienti 2012).

Mrk 421 does not show significant correlated variability when analysed as part of the uniform sample described in Section 2. Furthermore, neither the radio nor the gamma-ray PSD can be fitted so the population averages were used as described in Section 3. To include the radio and gamma-ray flares, we extended the light curves beyond the period used for the uniform sample (Section 2). We repeated the analysis using these extended light curves and found  $0.6 < \beta_{\text{radio}} < 2.0$ , with best-fitting value 1.8, and  $1.6 < \beta_\gamma < 2.1$ , with best-fitting value 1.6. The cross-correlation peak at  $-40 \pm 9$  d has a significance between 96.16 and 99.99 per cent depending on the PSD model. The significance obtained using the best-fitting PSD models is 98.96 per cent (Fig. 2). This result should be treated with caution: extending the data set after noticing the flare is ‘a posteriori’ statistics, and as such cannot be used to make inferences about the rate at which significant correlations are found in the general blazar population.

#### 6 INTERPRETATION OF THE TIME DELAYS

The duration of the correlated events is typically a few hundred days, and a detailed model is needed to understand the relationship between the lags and the location of the emission regions. Here, we ignore the flare duration and tentatively interpret the delays using a model in which a moving emission region, confined to the jet, produces the radio and gamma-ray activity. This region moves outwards at the bulk jet speed  $\beta c$  (Fig. 3), and corresponds to the moving disturbances observed with very long baseline interferometry (VLBI). The gamma-ray flare becomes observable at distance  $d_\gamma$  from the central engine, after crossing the surface of unit gamma-ray opacity (gamma-sphere; Blandford & Levinson 1995). Likewise, the radio flare becomes observable upon crossing the surface of unit radio opacity (‘radio core’), at distance  $d_{\text{core}}$  from the central engine (Blandford & Konigl 1979).

The time lag between these wavebands provides an estimate of the interval between the emergence of gamma-ray and radio radiation. The distance travelled by the emission region between the peaks in gamma-ray and radio emission is

$$d = \frac{\Gamma D \beta c \Delta t}{(1+z)}, \quad (1)$$

<sup>4</sup> This is consistent with the threshold of 97.56 per cent when the 0.13 per cent uncertainty is considered as shown in Table 1.

**Table 1.** Cross-correlation significance results.

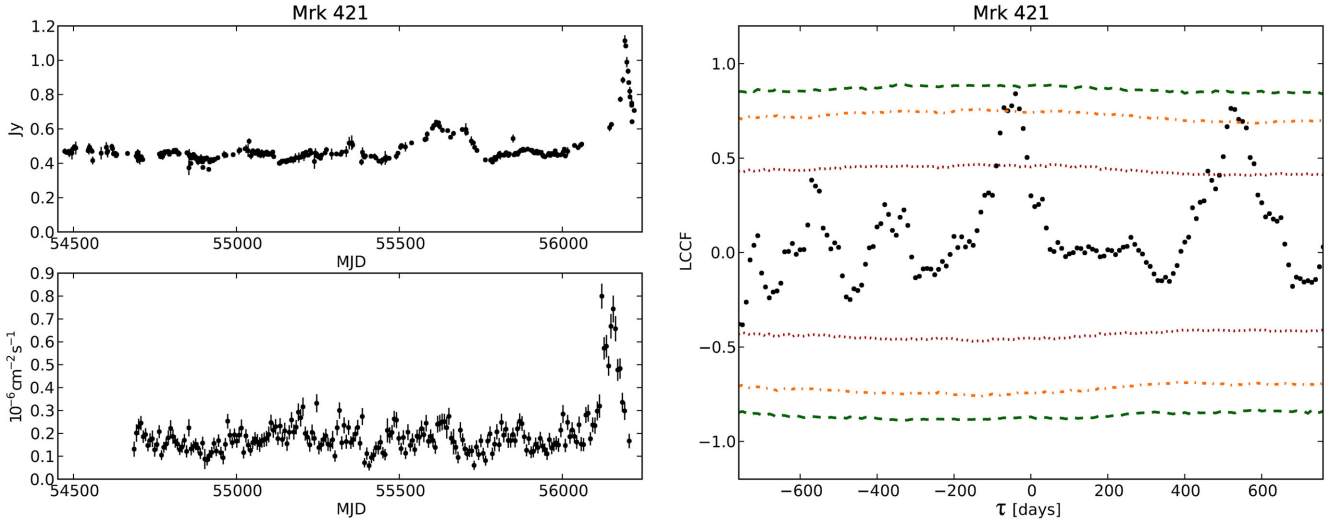
Source name	Name 2FGL	Class optical <sup>(a)</sup>	Class SED <sup>(a)</sup>	$z$	$\beta_{\text{radio}}^{\text{best}}$ (b)	$\beta_{\text{radio}}^{\text{low}}$ (b)	$\beta_{\text{radio}}^{\text{up}}$ (b)	$\beta_{\gamma}^{\text{best}}$ (b)	$\beta_{\gamma}^{\text{low}}$ (b)	$\beta_{\gamma}^{\text{up}}$ (b)	$\tau$ (d)	DCF (c)	Sig. (per cent) (c)	Sig <sub>low</sub> (per cent) (c)	Sig <sub>up</sub> (per cent) (c)	Sig <sub>unc</sub> (per cent) (c)	Sig <sub><math>\sigma</math></sub> (c)	Flags (d)
4C +01.02	J0108.6+0135	FSRQ	LSP	2.099	2.3	–	–	1.6	–	–	$-340 \pm 16$	0.33	58.64	–	–	0.49	0.82	ng
S2 0109+22	J0112.1+2245	BL Lac	ISP	0.265	2.0	1.4	2.4	0.9	0.0	1.8	$-380 \pm 13$	0.24	59.63	36.05	94.45	0.48	0.84	–
4C 31.03	J0112.8+3208	FSRQ	LSP	0.603	2.3	–	–	1.6	–	–	$-190 \pm 12$	0.36	54.65	–	–	0.5	0.75	tg
OC 457	J0136.9+4751	FSRQ	LSP	0.859	1.6	1.4	1.9	1.6	–	–	$-230 \pm 14$	0.62	95.75	92.92	97.76	0.19	2.03	–
PKS 0215+015	J0217.9+0143	FSRQ	LSP	1.721	2.3	–	–	1.6	–	–	$-60 \pm 15$	0.38	65.75	–	–	0.46	0.95	–
S4 0218+35	J0221.0+3555	FSRQ	–	0.944	2.3	–	–	1.6	–	–	$-190 \pm 12$	0.51	93.08	–	–	0.25	1.82	ng
3C 66A	J0222.6+4302	BL Lac	ISP	–	1.9	0.4	2.5	0.6	0.2	1.2	$460 \pm 14$	0.27	81.16	60.78	99.96	0.39	1.32	–
4C +28.07	J0237.8+2846	FSRQ	LSP	1.206	2.7	2.5	3.0	1.6	–	–	$-140 \pm 13$	0.63	83.59	81.78	85.31	0.37	1.39	–
AO 0235+164	J0238.7+1637	BL Lac	LSP	0.94	2.3	–	–	0.1	0.0	1.0	$-150 \pm 8$	0.91	99.99	99.99	99.99	–	3.89	–
NGC 1275	J0319.8+4130	Radio Gal	...	0.018	2.3	–	–	1.6	1.1	2.2	$-420 \pm 13$	0.59	81.54	73.56	93.0	0.39	1.33	–
PKS 0420–01	J0423.2–0120	FSRQ	LSP	0.916	2.5	2.2	2.8	1.6	–	–	$-20 \pm 16$	0.49	76.65	75.2	79.57	0.42	1.19	–
PKS 0440–00	J0442.7–0017	FSRQ	LSP	0.844	2.3	–	–	0.7	0.1	2.3	$420 \pm 32$	0.22	59.27	31.11	78.29	0.47	0.83	–
TXS 0506+056	J0509.4+0542	BL Lac	ISP	0.0	2.2	0.6	2.7	1.6	–	–	$450 \pm 15$	0.25	61.54	58.89	96.86	0.5	0.87	tg, ng
B2 0716+33	J0719.3+3306	FSRQ	LSP	0.779	2.3	–	–	1.6	–	–	$140 \pm 8$	0.61	90.05	–	–	0.31	1.65	–
S5 0716+71	J0721.9+7120	BL Lac	ISP	0.0	2.3	–	–	1.9	1.4	2.3	$-200 \pm 11$	0.37	44.89	39.86	55.97	0.49	0.6	–
4C +14.23	J0725.3+1426	FSRQ	LSP	1.038	2.3	–	–	0.5	0.1	1.0	$150 \pm 13$	0.19	61.5	43.28	76.51	0.48	0.87	–
PKS 0736+01	J0739.2+0138	FSRQ	LSP	0.189	2.3	–	–	1.6	–	–	$-360 \pm 15$	0.5	79.7	–	–	0.39	1.27	ng
GB6 J0742+5444	J0742.6+5442	FSRQ	LSP	0.723	1.9	0.6	2.9	1.6	–	–	$-190 \pm 9$	0.69	92.09	83.89	99.99	0.27	1.76	–
PKS 0805–07	J0808.2–0750	FSRQ	LSP	1.837	2.0	1.6	2.5	0.5	0.1	1.1	$-150 \pm 16$	0.59	99.52	88.86	99.99	0.07	2.82	–
PKS 0829+046	J0831.9+0429	BL Lac	LSP	0.174	1.9	0.6	2.3	1.6	–	–	$150 \pm 16$	0.42	81.09	75.95	99.89	0.4	1.31	ng
4C +71.07	J0841.6+7052	FSRQ	LSP	2.218	2.3	–	–	1.6	–	–	$210 \pm 11$	0.63	91.74	–	–	0.28	1.74	tg, ng
OJ 287	J0854.8+2005	BL Lac	ISP	0.306	2.3	–	–	1.6	–	–	$-70 \pm 16$	0.38	62.48	–	–	0.48	0.89	ng
PKS 0906+01	J0909.1+0121	FSRQ	LSP	1.026	2.3	–	–	1.6	–	–	$510 \pm 16$	0.39	68.85	–	–	0.48	1.01	–
S4 0917+44	J0920.9+4441	FSRQ	LSP	2.189	2.3	–	–	1.6	0.8	2.1	$-460 \pm 12$	0.49	70.51	62.12	92.86	0.48	1.05	tr, tg, nr, ng
MG2 J101241+2439	J1012.6+2440	FSRQ	–	1.805	2.3	–	–	1.6	–	–	$490 \pm 49$	0.57	99.51	–	–	0.07	2.81	–
4C +01.28	J1058.4+0133	BL Lac	LSP	0.888	2.3	–	–	1.6	–	–	$510 \pm 15$	0.6	93.42	–	–	0.25	1.84	ng
Mrk 421	J1104.4+3812	BL Lac	HSP	0.031	2.3	–	–	1.6	–	–	$-500 \pm 10$	0.39	73.78	–	–	0.43	1.12	ng
PKS 1124–186	J1126.6–1856	FSRQ	LSP	1.048	2.0	1.6	2.4	1.6	–	–	$10 \pm 11$	0.76	97.62	95.88	99.2	0.15	2.26	–
Ton 599	J1159.5+2914	FSRQ	LSP	0.725	2.1	1.8	2.6	1.0	0.5	1.6	$-70 \pm 18$	0.42	79.05	55.61	95.39	0.39	1.25	–
IES 1215+303	J1217.8+3006	BL Lac	HSP	0.13	2.3	–	–	1.6	–	–	$120 \pm 9$	0.5	91.88	–	–	0.27	1.74	ng
4C +21.35	J1224.9+2122	FSRQ	LSP	0.434	2.4	0.9	2.7	0.4	0.2	0.8	$-380 \pm 10$	0.59	99.78	96.51	99.99	0.05	3.06	–
MG1 J123931+0443	J1229.1+0202	FSRQ	LSP	0.158	2.2	0.6	2.8	0.8	0.4	1.1	$-240 \pm 16$	0.41	86.32	68.08	99.99	0.33	1.49	–
3C 273	J1239.5+0443	FSRQ	LSP	1.761	2.3	–	–	1.6	–	–	$-50 \pm 15$	0.67	89.01	–	–	0.3	1.6	–
3C 279	J1256.1–0547	FSRQ	LSP	0.536	2.4	2.0	2.7	1.6	1.2	2.0	$190 \pm 10$	0.47	65.03	54.86	80.94	0.48	0.94	–
OP 313	J1310.6+3222	FSRQ	LSP	0.997	2.2	1.9	2.4	1.6	–	–	$500 \pm 74$	0.32	49.79	47.75	54.35	0.5	0.67	–
GB 1310+487	J1312.8+4828	FSRQ	LSP	0.501	2.3	–	–	0.3	0.0	1.0	$-350 \pm 15$	0.36	93.09	77.42	96.31	0.25	1.82	–
PKS 1329–049	J1332.0–0508	FSRQ	LSP	2.15	2.2	1.4	2.9	0.3	0.1	0.8	$-90 \pm 15$	0.51	99.56	90.36	99.98	0.07	2.85	–
B3 1343+451	J1345.4+4453	FSRQ	LSP	2.534	2.1	0.6	2.6	1.6	–	–	$30 \pm 13$	0.51	67.5	62.53	99.88	0.48	0.98	–
PKS 1424+240	J1427.0+2347	BL Lac	HSP	0.0	2.3	–	–	1.6	–	–	$110 \pm 13$	0.45	95.59	–	–	0.2	2.01	tr, tg, nr, ng
PKS 1502+106	J1504.3+1029	FSRQ	LSP	1.839	2.5	2.2	2.8	1.6	–	–	$-40 \pm 13$	0.87	98.09	97.54	98.7	0.13	2.34	–



Table 1 – continued

Source name	Name 2FGL	Class optical <sup>(a)</sup>	Class SED <sup>(a)</sup>	$z$ <sup>(a)</sup>	$\beta_{\text{radio}}^{\text{best}}$ <sup>(b)</sup>	$\beta_{\text{radio}}^{\text{low}}$ <sup>(b)</sup>	$\beta_{\text{radio}}^{\text{up}}$ <sup>(b)</sup>	$\beta_{\gamma}^{\text{best}}$ <sup>(b)</sup>	$\beta_{\gamma}^{\text{low}}$ <sup>(b)</sup>	$\beta_{\gamma}^{\text{up}}$ <sup>(b)</sup>	$\tau$ <sup>(d)</sup>	DCF <sup>(c)</sup>	Sig. <sup>(c)</sup> (per cent)	Sig <sub>low</sub> <sup>(c)</sup> (per cent)	Sig <sub>up</sub> <sup>(c)</sup> (per cent)	Sig <sub>unc</sub> <sup>(c)</sup> (per cent)	Sig <sub><math>\sigma</math></sub> <sup>(c)</sup>	Flags <sup>(d)</sup>
PKS 1510–08	J1512.8–0906	FSRQ	LSP	0.36	2.3	1.6	2.9	1.6	–	–	$-60 \pm 6$	0.65	83.59	78.01	92.58	0.37	1.39	–
B2 1520+31	J1522.1+3144	FSRQ	LSP	1.484	2.3	–	–	–	0.7	1.0	$350 \pm 8$	0.45	95.65	90.11	99.0	0.2	2.02	–
GB6 J1542+6129	J1542.9+6129	BL Lac	ISP	0.0	2.3	–	–	–	1.6	–	$360 \pm 16$	0.38	78.75	–	–	0.41	1.25	tg, ng
PG 1553+113	J1555.7+1111	BL Lac	HSP	0.0	2.3	–	–	–	1.6	–	$530 \pm 17$	0.43	99.69	–	–	0.06	2.96	tr, tg, nr, ng
4C +38.41	J1635.2+3810	FSRQ	LSP	1.813	2.1	1.4	2.9	1.5	1.1	1.8	$500 \pm 8$	0.79	96.28	90.24	99.99	0.2	2.08	–
Mrk 501	J1653.9+3945	BL Lac	HSP	0.034	2.3	–	–	–	1.6	–	$-480 \pm 12$	0.5	98.11	–	–	0.13	2.35	tg, ng
B3 1708+433	J1709.7+4319	FSRQ	LSP	1.027	2.3	–	–	–	1.6	–	$-50 \pm 12$	0.59	80.86	–	–	0.39	1.31	–
PKS 1730–13	J1733.1–1307	FSRQ	LSP	0.902	2.0	1.5	2.4	1.6	–	–	$-260 \pm 14$	0.5	73.67	68.25	83.55	0.44	1.12	tg
S4 1749+70	J1748.8+7006	BL Lac	ISP	0.77	2.2	1.4	2.7	0.4	0.0	1.1	$230 \pm 10$	0.55	99.48	87.86	99.99	0.07	2.79	–
S5 1803+784	J1800.5+7829	BL Lac	LSP	0.68	2.3	–	–	–	0.4	0.0	$-430 \pm 11$	0.47	98.43	89.17	99.89	0.12	2.42	tg
4C +56.27	J1824.0+5650	BL Lac	LSP	0.664	1.9	0.4	2.9	1.6	–	–	$-240 \pm 11$	0.46	80.36	74.26	99.99	0.39	1.29	tg, ng
B2 1846+32A	J1848.5+3216	FSRQ	LSP	0.798	2.2	1.9	2.7	1.6	–	–	$-300 \pm 12$	0.53	65.95	61.37	69.83	0.47	0.95	–
S4 1849+67	J1849.4+6706	FSRQ	LSP	0.657	1.9	0.8	2.5	0.6	0.2	1.2	$-40 \pm 10$	0.38	90.61	61.42	99.91	0.3	1.68	–
IES 1959+650	J2000.0+6509	BL Lac	HSP	0.047	2.3	–	–	–	1.6	–	$-80 \pm 13$	0.41	90.97	–	–	0.3	1.69	tg, ng
PKS 2023–07	J2025.6–0736	FSRQ	LSP	1.388	2.3	–	–	–	1.6	–	$130 \pm 12$	0.55	72.89	–	–	0.44	1.1	–
OX 169	J2143.5+1743	FSRQ	LSP	0.211	2.3	–	–	–	0.0	0.5	$-320 \pm 11$	0.34	99.04	89.26	98.96	0.1	2.59	–
BL Lacertae	J2202.8+4216	BL Lac	ISP	0.069	2.1	0.9	2.7	2.0	1.5	2.4	$-160 \pm 14$	0.71	85.27	72.37	99.99	0.36	1.45	–
PKS 2201+171	J2203.4+1726	FSRQ	LSP	1.076	2.0	1.5	2.3	1.6	–	–	$530 \pm 10$	0.58	93.29	92.2	97.46	0.26	1.83	ng
PKS 2227–08	J2229.7–0832	FSRQ	LSP	1.56	2.8	2.4	3.1	1.6	–	–	$310 \pm 14$	0.51	80.95	79.82	83.36	0.41	1.31	ng
CTA 102	J2232.4+1143	FSRQ	LSP	1.037	2.4	1.7	2.8	1.6	–	–	$-430 \pm 8$	0.42	55.1	51.02	66.17	0.5	0.76	–
B2 2234+28A	J2236.4+2828	BL Lac	LSP	0.795	1.9	0.6	2.3	1.6	–	–	$110 \pm 14$	0.35	63.42	58.81	99.39	0.48	0.9	–
3C 454.3	J2253.9+1609	FSRQ	LSP	0.859	2.4	1.9	2.6	1.6	–	–	$-80 \pm 18$	0.55	71.96	70.12	78.46	0.46	1.08	–
<b>B2 2308+34</b>	<b>J2311.0+3425</b>	<b>FSRQ</b>	<b>LSP</b>	<b>1.817</b>	<b>2.1</b>	<b>0.6</b>	<b>2.7</b>	<b>0.2</b>	<b>0.0</b>	<b>0.9</b>	<b><math>-120 \pm 14</math></b>	<b>0.73</b>	<b>99.99</b>	<b>99.33</b>	<b>99.99</b>	<b>–</b>	<b>3.89</b>	<b>–</b>

(a): Optical class, SED class, and redshifts from Ackermann et al. (2011b).  $z = 0.0$  indicates that redshift could not be evaluated with available optical spectrum. (b):  $\beta_{\text{waveband}}^{\text{best/low/up}}$ : PSD power-law index for given 'waveband': 'best' for best fit, 'low' for lower limit and 'up' for upper limit.  $\tau$ : radio/gamma-ray time lag, negative values indicate radio lags gamma-ray variations. DCF: discrete correlation function estimate. Sig.: significance of the correlation. Sig<sub>low/up/unc/ $\sigma$</sub> : significance lower limit, upper limit, uncertainty, and significance in units of standard deviations. (c):  $\tau$ : radio/gamma-ray time lag, negative values indicate radio lags gamma-ray variations. DCF: discrete correlation function estimate. Sig.: significance of the correlation. Sig<sub>low/up/unc/ $\sigma$</sub> : significance lower limit, upper limit, uncertainty, and significance in units of standard deviations. (d): lags are: noisy light curves in radio (nr) and gamma-ray band (ng); trends in radio (tr) and gamma-ray band (tg) (see the text).



**Figure 2.** Light curves (left) and cross-correlation (right) for Mrk 421. The most significant peak is at  $-40 \pm 9$  d with 98.96 per cent significance. Colours and line styles as in Fig. 1.

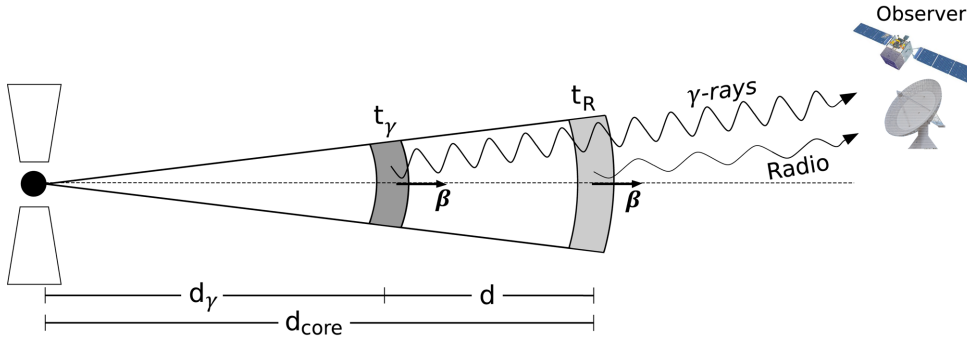


**Figure 3.** Model for the interpretation of time lags. The central engine launches a jet in which disturbances propagate at speed  $\beta c$ . A moving disturbance (shaded area) is depicted at two times:  $t_\gamma$  at which gamma-ray emission peaks and  $t_R$  for the peak of radio emission when crossing the radio core.

where  $\Gamma$  is the bulk Lorentz factor,  $D$  is the Doppler factor,  $\Delta t$  is the time lag, and  $z$  is the redshift (Pushkarev et al. 2010). The apparent jet speed,  $\beta_{\text{app}}$ , is determined from VLBI monitoring and the Doppler factor is estimated from the radio variability time-scale (Hovatta et al. 2009). Doppler factors from this method have a typical 27 per cent scatter for individual flares in a given source, which we adopt as the uncertainty in  $D$ . From  $D$  and  $\beta_{\text{app}}$ , we obtain  $\Gamma$  and the jet viewing angle  $\theta$  (e.g. Hovatta et al. 2009).  $\beta_{\text{app}}$  and  $D$  are not measured simultaneously with our observations; we assume them constant in our calculations.

We estimate  $d_\gamma = d_{\text{core}} - d$ , where  $d_{\text{core}}$  is determined from VLBI measurements of the angular diameter of the radio core,  $\theta_{\text{core}}$ . This, plus the intrinsic opening angle,  $\alpha_{\text{int}}$ , and redshift, gives

$$d_{\text{core}} \sim \frac{(\theta_{\text{core}}/2)d_A}{\tan(\alpha_{\text{int}}/2)}, \quad (2)$$

where  $d_A$  is the angular diameter distance, obtained assuming a  $\Lambda$  cold dark matter cosmology with  $H_0 = 70 \text{ km s}^{-1} \text{ Mpc}^{-1}$ ,  $\Omega_m = 0.27$ , and  $\Omega_\Lambda = 0.73$  (Komatsu et al. 2011). Equation (2) is only valid for a conical jet with vertex at the central engine. However, there is observational evidence for collimation in the M87 jet, which we use as a prototype for the collimation properties of other sources where no such information is available. Asada & Nakamura (2012) model the jet profile as  $z_{\text{jet}} \propto r^a$ , where  $r$  is the radius of the jet cross-section at distance  $z_{\text{jet}}$  from the central engine,

and found  $a = 1.73 \pm 0.05$  for  $z_{\text{jet}} \lesssim 2.5 \times 10^5 r_s$ , where  $r_s$  is the Schwarzschild radius, and  $a = 0.96 \pm 0.1$  at distances outside the collimation zone. Assuming that the radio core is in the collimation zone and setting  $r$  and  $dr/dz_{\text{jet}}$  equal for both models

$$d_{\text{core}}(\text{coll}) = \frac{1}{a} d_{\text{core}}(\text{cone}). \quad (3)$$

This model reduces our estimate of  $d_{\text{core}}$  by a factor of 1.73. We thus obtain lower and upper limits on  $d_{\text{core}}$  using these alternatives.

Detailed distance estimates are provided below for AO 0235+164, the highest significance case, and Mrk 421 which has the sharpest cross-correlation peak. For PKS 1502+106, only the final result is given as a reference, and for B2 2308+34, there are no published VLBI results which makes it impossible to provide a constraint. A summary of the results for AO 0235+164 is given in Table 2.

### 6.1 Estimation of $d$

For AO 0235+164, we have  $D = 24$  (Hovatta et al. 2009) but no  $\beta_{\text{app}}$  since its jet is unresolved in 15 GHz VLBI (Lister et al. 2009). We assume that the source is seen at the critical angle,  $\theta_{\text{cr}} = \theta = 2.4$ . We obtain  $d = 37.3 \pm 22.8 \text{ pc}$  for  $\tau = -150 \pm 8 \text{ d}$ , the most significant time lag, and  $d = 7.5 \pm 5.3 \text{ pc}$  for the peak at  $\tau = -30 \pm 9 \text{ d}$ . For comparison, if we use  $\theta = \theta_{\text{cr}}/2$ , we obtain  $d = 20 \pm 15 \text{ pc}$

**Table 2.** Results of the distance estimates for the different jet components in the most significant case.<sup>a</sup>

Source	$d$ (pc)	$d_{\text{core(coll)}}$ (pc)	$d_{\text{core(cone)}}$ (pc)	$d_{\gamma(\text{coll})}$ (pc)	$d_{\gamma(\text{cone})}$ (pc)
AO 0235+164, $\tau = -150 \pm 8$ d	$37 \pm 23$	$\gtrsim 23 \pm 6$	$\gtrsim 40 \pm 11$	$\gtrsim -14 \pm 24^b$	$\gtrsim 3 \pm 25$
AO 0235+164, $\tau = -30 \pm 9$ d	$8 \pm 5$	$\gtrsim 23 \pm 6$	$\gtrsim 40 \pm 11$	$\gtrsim 15 \pm 8$	$\gtrsim 32 \pm 12$

<sup>a</sup>Columns –  $d$ : distance travelled by the emission region between the peaks in gamma-ray and radio emission.  $d_{\text{core(coll/cone)}}$ : distance between radio core and central engine with and without collimation.  $d_{\gamma(\text{coll/cone})}$ : location of the peak of the gamma-ray emission with respect to the central engine.

<sup>b</sup>The negative value is an artefact produced by the large measurement errors.

( $3.9 \pm 3.2$  pc) for the peak at  $-150$  d ( $-30$  d). If  $\theta = 0$ , we obtain  $d = 18 \pm 12$  pc ( $3.7 \pm 2.6$  pc).

For Mrk 421, we use a preliminary variability Doppler factor for the recent flare of  $D = 4$  (Richards et al. 2013).  $\beta_{\text{app}}$  is uncertain, with jet components consistent with being stationary (Lico et al. 2012). Assuming  $\theta \sim 4^\circ$  (Lico et al. 2012 estimate  $2^\circ$ – $5^\circ$ ), then  $\Gamma \sim 2.2$  and  $d \sim 0.2$  pc. It is difficult to estimate uncertainties because of the limited knowledge of the jet properties.

## 6.2 Estimation of $d_{\text{core}}$

The core angular size (full width at half-maximum) has been measured for AO 0235+164 ( $\theta_{\text{core}} = 0.21 \pm 0.06$  mas; Lister et al. 2009). Here, we have averaged multiple epochs, with uncertainties estimated from their scatter. For Mrk 421, we use  $\theta_{\text{core}} = 0.16$  mas (Kovalev et al. 2005), assuming an error of 0.05 mas, the angular resolution of the observations.

For the intrinsic opening angle, we use  $\alpha_{\text{int}} \lesssim 2.4$  for AO 0235+164, which is the critical angle upper limit from Section 6.1, consistent with what is used by Agudo et al. (2011b). For Mrk 421, we adopt  $\alpha_{\text{int}} = 2.4$ , the mean value for BL Lacs from Pushkarev et al. (2009).

The estimates of  $d_{\text{core}}$  for a conical jet are  $\gtrsim 40 \pm 11$  pc for AO 0235+164 and about 2.4 pc for Mrk 421. For a collimated jet, we obtain  $d_{\text{core}} \gtrsim 23 \pm 6$  pc for AO 0235+164, and about 1.4 pc for Mrk 421.

Similar estimates can be made for PKS 1502+106, resulting in  $d_{\gamma}$  of  $22 \pm 15$  pc for a conical jet and  $12 \pm 9$  pc for the collimated jet case.

## 7 CONCLUSIONS

Out of 41 sources for which a detailed correlation analysis is possible, three show correlations with larger than  $2.25\sigma$  significance, with only one of those larger than  $3\sigma$ . In all cases, radio variations lag behind gamma-ray variations, suggesting that the gamma-ray emission originates upstream of the radio emission. We use a simple model to tentatively estimate the distance from the black hole at which the gamma-ray emission is produced. Due to correlation peak breadth and uncertain jet parameters, these estimates have large uncertainties. In particular, AO 0235+164 shows two peaks in its cross-correlation with comparable amplitude and equivalent significance, leading to a highly uncertain location for the gamma-ray emission site.

These results show that correlations between radio and gamma-ray light curves of blazars are only found in a minority of the sources over a 4 yr period. This could indicate a complex multiwavelength connection not detectable with the tools and data we use. A better understanding of this connection requires continuation of the OVRO and *Fermi* monitoring and will benefit from the addition of

polarization and other wavebands and methods that provide additional information.

## ACKNOWLEDGEMENTS

We thank Russ Keeney for his support at OVRO. The OVRO programme is supported in part by NASA grants NNX08AW31G and NNX11A043G and NSF grants AST-0808050 and AST-1109911. TH was supported by the Jenny and Antti Wihuri foundation and Academy of Finland project number 267324. Support from MPIFR for upgrading the OVRO 40 m telescope receiver is acknowledged. WM thanks Jeffrey Scargle, James Chiang, Stefan Larsson, and Iosif Papadakis for discussions. The National Radio Astronomy Observatory is a facility of the National Science Foundation operated under cooperative agreement by Associated Universities, Inc. The *Fermi*-LAT Collaboration acknowledges support from a number of agencies and institutes for both development and the operation of the LAT as well as scientific data analysis. These include NASA and DOE in the United States, CEA/Irfu and IN2P3/CNRS in France, ASI and INFN in Italy, MEXT, KEK, and JAXA in Japan, and the K. A. Wallenberg Foundation, the Swedish Research Council, and the National Space Board in Sweden. Additional support from INAF in Italy and CNES in France for science analysis during the operations phase is also gratefully acknowledged. We thank the anonymous referee for constructive comments that greatly improved the presentation of some sections of this paper.

## REFERENCES

- Abdo A. A. et al., 2010a, *Nature*, 463, 919
- Abdo A. A. et al., 2010b, *ApJ*, 715, 429
- Abdo A. A. et al., 2010c, *ApJ*, 722, 520
- Abdo A. A. et al., 2011, *ApJ*, 730, 101
- Ackermann M. et al., 2011a, *ApJ*, 741, 30
- Ackermann M. et al., 2011b, *ApJ*, 743, 171
- Agudo I. et al., 2011a, *ApJ*, 726, L13
- Agudo I. et al., 2011b, *ApJ*, 735, L10
- Arévalo P., Uttley P., Kaspi S., Breedt E., Lira P., McHardy I. M., 2008, *MNRAS*, 389, 1479
- Asada K., Nakamura M., 2012, *ApJ*, 745, L28
- Atwood W. B. et al., 2009, *ApJ*, 697, 1071
- Baars J. W. M., Genzel R., Pauliny-Toth I. I. K., Witzel A., 1977, *A&A*, 61, 99
- Blandford R. D., Konigl A., 1979, *ApJ*, 232, 34
- Blandford R. D., Levinson A., 1995, *ApJ*, 441, 79
- Błażejowski M., Sikora M., Moderski R., Madejski G. M., 2000, *ApJ*, 545, 107
- Chatterjee R. et al., 2008, *ApJ*, 689, 79
- D’Ammando F., Orienti M., 2012, *Astron. Telegram*, 4261, 1
- Dermer C. D., Schlickeiser R., 1993, *ApJ*, 416, 458
- Edelson R. A., Krolik J. H., 1988, *ApJ*, 333, 646
- Edelson R. et al., 1995, *ApJ*, 438, 120



- Fuhrmann L. et al., 2014, MNRAS, 441, 1899  
 Healey S. E. et al., 2008, ApJS, 175, 97  
 Hovatta T., Valtaoja E., Tornikoski M., Lähteenmäki A., 2009, A&A, 494, 527  
 Hovatta T., Richards J. L., Aller M. F., Aller H. D., Max-Moerbeck W., Pearson T. J., Readhead A. C. S., 2012, Astron. Telegram, 4451, 1  
 Hufnagel B. R., Bregman J. N., 1992, ApJ, 386, 473  
 Jones T. W., O'dell S. L., Stein W. A., 1974, ApJ, 188, 353  
 Jorstad S. G., Marscher A. P., Mattox J. R., Aller M. F., Aller H. D., Wehrle A. E., Bloom S. D., 2001, ApJ, 556, 738  
 Komatsu E. et al., 2011, ApJS, 192, 18  
 Kovalev Y. Y. et al., 2005, AJ, 130, 2473  
 Kovalev Y. Y. et al., 2009, ApJ, 696, L17  
 Lico R. et al., 2012, A&A, 545, A117  
 Lister M. L. et al., 2009, AJ, 138, 1874  
 Mahony E. K., Sadler E. M., Murphy T., Ekers R. D., Edwards P. G., Massardi M., 2010, ApJ, 718, 587  
 Mannheim K., Biermann P. L., 1992, A&A, 253, L21  
 Marscher A. P. et al., 2008, Nature, 452, 966  
 Mattox J. R. et al., 1996, ApJ, 461, 396  
 Max-Moerbeck W., Richards J. L., Hovatta T., Pavlidou V., Pearson T. J., Readhead A. C. S., 2014, MNRAS, preprint ([arXiv:1408.6265](https://arxiv.org/abs/1408.6265))  
 Nieppola E., Tornikoski M., Valtaoja E., León-Tavares J., Hovatta T., Lähteenmäki A., Tammi J., 2011, A&A, 535, A69  
 Nolan P. L. et al., 2012, ApJS, 199, 31  
 Pavlidou V. et al., 2012, ApJ, 751, 149  
 Peterson B. M., Wanders I., Horne K., Collier S., Alexander T., Kaspi S., Maoz D., 1998, PASP, 110, 660  
 Pushkarev A. B., Kovalev Y. Y., Lister M. L., Savolainen T., 2009, A&A, 507, L33  
 Pushkarev A. B., Kovalev Y. Y., Lister M. L., 2010, ApJ, 722, L7  
 Richards J. L. et al., 2011, ApJS, 194, 29  
 Richards J. L. et al., 2013, Eur. Phys. J. Web Conf., 61, 4010  
 Sikora M., Begelman M. C., Rees M. J., 1994, ApJ, 421, 153  
 Timmer J., Koenig M., 1995, A&A, 300, 707  
 Uttley P., McHardy I. M., Papadakis I. E., 2002, MNRAS, 332, 231  
 Uttley P., Edelson R., McHardy I. M., Peterson B. M., Markowitz A., 2003, ApJ, 584, L53  
 von Montigny C. et al., 1995, ApJ, 440, 525  
 Welsh W. F., 1999, PASP, 111, 1347

This paper has been typeset from a  $\text{\TeX}/\text{\LaTeX}$  file prepared by the author.